Reinforcement of DC Electrified Railways by a Modular Battery Energy Storage System

Erick Matheus da Silveira Brito, Philippe Ladoux, Joseph Fabre, Benoit Sonier

electronics

MDPI

Article

Reinforcement of DC Electrified Railways by a Modular Battery Energy Storage System

Erick Matheus da Silveira Brito [1,2,*], Philippe Ladoux [1], Joseph Fabre [3] and Benoit Sonier [4]

[1] Laboratory of Plasma and Energy Conversion (LAPLACE), University of Toulouse, 31071 Toulouse, France; ladoux@laplace.univ-tlse.fr
[2] Institute of Exact and Technological Sciences, Federal University of Viçosa, Florestal 35690-000, Brazil
[3] Société de Construction des Lignes Électriques-Systèmes pour Ferroviaire et Énergie (SCLE-SFE), 31204 Toulouse, France; joseph.fabre@scle.fr
[4] Société Nationale des Chemins de Fer Français (SNCF-Réseau), 93574 Saint Denis, France; benoit.sonier@reseau.sncf.fr
* Correspondence: erick.brito@ufv.br

Abstract: DC railway electrification was deployed at the beginning of the 20th century in several countries in Europe. Today, this power system is no longer adapted to the demands of increased rail traffic. Due to the relatively low voltage level, the current consumed by the trains reaches several kAs. So, in the worst case, the locomotives cannot operate at their rated power due to the voltage drop along the contact line. Conventional solutions to reduce the voltage drop consist of increasing the cross-section of overhead lines or reducing the length of sectors by installing additional substations. Nevertheless, these solutions are expensive and not always feasible. The implementation of a Modular Battery Energy Storage System (MBESS) can be an alternative solution to reinforce the railway power supply. This paper first presents an MBESS based on elementary blocks associating Full-SiC Isolated DC-DC converter and battery racks. The electrical models of a railway sector and an elementary block are described, and simulations are performed considering real railroad traffic on two sectors of the French National Rail Network, electrified at 1.5 kV. The results show that the installation of an MBESS in the railway sector boosts the locomotive's voltage while also increasing overall system efficiency.

Keywords: rail transportation power systems; energy storage; power electronics; batteries

Citation: da Silveira Brito, E.M.; Ladoux, P.; Fabre, J.; Sonier, B. Reinforcement of DC Electrified Railways by a Modular Battery Energy Storage System. *Electronics* **2024**, *13*, 1933. https://doi.org/10.3390/electronics13101933

Academic Editor: Krzysztof Zboiński

Received: 13 April 2024
Revised: 3 May 2024
Accepted: 11 May 2024
Published: 15 May 2024

1. Introduction

In the European Union (EU), four railway electrification systems are mainly used: DC, at 1.5 kV or 3 kV, Medium Voltage AC (MVAC) of 15 kV at the special frequency of 16.7 Hz and 25 kV at the standard line frequency of 50 Hz [1]. The first two systems were introduced at the beginning of the 20th century. The last one was developed after World War II. From that moment, the countries that had not yet electrified their railway lines chose the 25 kV/50 Hz system. The other electrification systems, already in place, were kept and even extended during the second half of the 20th century. Today, in the EU, 43% of electrified railway routes are powered by DC, 30% at 15 kV/16.7 Hz, and 27% at 25 kV/50 Hz [2].

Faced with the collective need to favor modes of transport that are more respectful of the environment, train traffic, for freight and passengers, is expected to increase in the years to come [3]. From the point of view of the railway network operator, an increase in traffic is only possible if a minimum contact-line voltage can be ensured to allow the locomotives to draw the power necessary to keep to their timetables [4]. Due to its relatively low voltage level, the DC electrification system is penalized by the level of current absorbed by the trains which can reach several kAs. Conventional solutions to reduce the voltage drop consist of increasing the cross-section of overhead lines or reducing the length of

sectors by installing new substations [5]. Additionally, paralleling stations (PS) at the middle of the sector can be added to reduce the contact-line resistance. Previous studies have demonstrated that the middle of the sector between two substations is the critical point in terms of voltage drop. Excluding the paralleling stations (since the majority of the DC railway lines already have a PS installed), the other solutions are expensive and not always feasible. As of 2014, several papers proposing a Medium Voltage DC (MVDC) electrification system were published [6–9]. In [10], it was demonstrated that a nominal contact-line voltage of 9 kV made it possible to obtain performances similar to those of 25 kV/50 Hz electrification system in terms of railroad traffic, substation spacing, and contact-line cross-section. Figure 1 illustrates a DC-electrified railway system. When the line is electrified at 1.5 kV, the distance between substations, referred to as D, is in the order of 10–20 km. Nevertheless, for a line electrified at 9 kV, the substations could be spaced approximately 50 km apart.

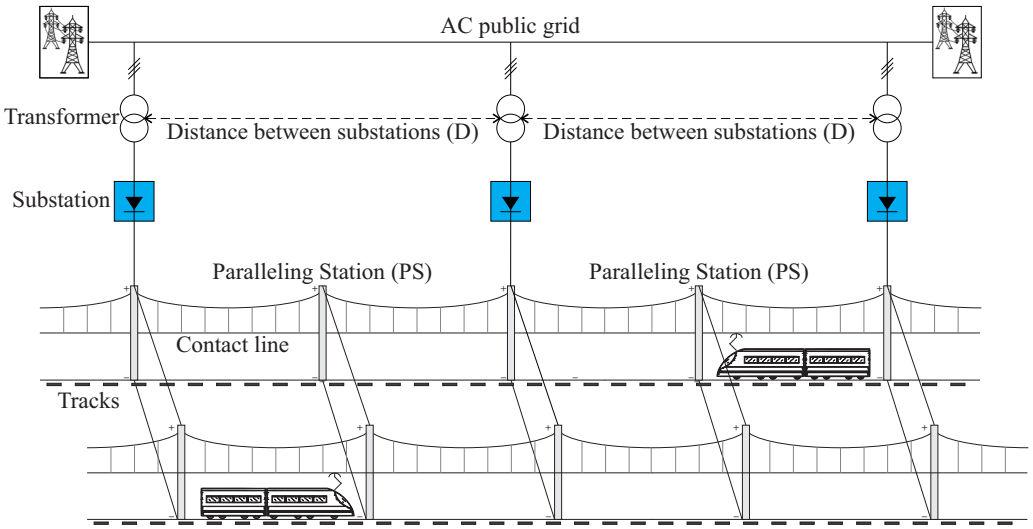

Figure 1. Representation of a DC electrified double-track railway system.

However, changing the voltage level to MVDC is challenging cost-wise. On the one hand, new rectifier groups have to be installed in substations and MVDC circuit breakers have to be developed. On the other hand, updating all the rolling stock traction converters is not a simple task even considering advances in high blocking-voltage semiconductors [10]. Therefore, the MVDC electrification system is considered only as a long-term solution. In the short term, several reinforcement solutions can be deployed. The principle of a three-wire DC power supply is illustrated in Figure 2. This solution can be considered as an intermediate stage in converting a classical DC power supply, e.g., 1.5 kV or 3 kV, to MVDC. MVDC rectifier groups are installed in existing substations and an additional feed-wire is deployed on the support posts of the contact line. Then DC/DC converters are implemented at the PS to reinforce the power supply and boost the voltage on the contact lines [11].

Other reinforcement solutions, also shown in Figure 2, rely on energy storage systems and renewable energy sources, e.g., photovoltaic (PV) systems, integrated with the DC power electrification lines [12–14]. Solutions involving battery energy storage systems (BESS) have gained attention in the last few years. Due to the environmental pressure, the road transportation sector is shifting from fossil fuels to more sustainable electric power. This demand drives advances and developments in battery technologies, creating more reliable, efficient, and less expensive solutions [15,16].

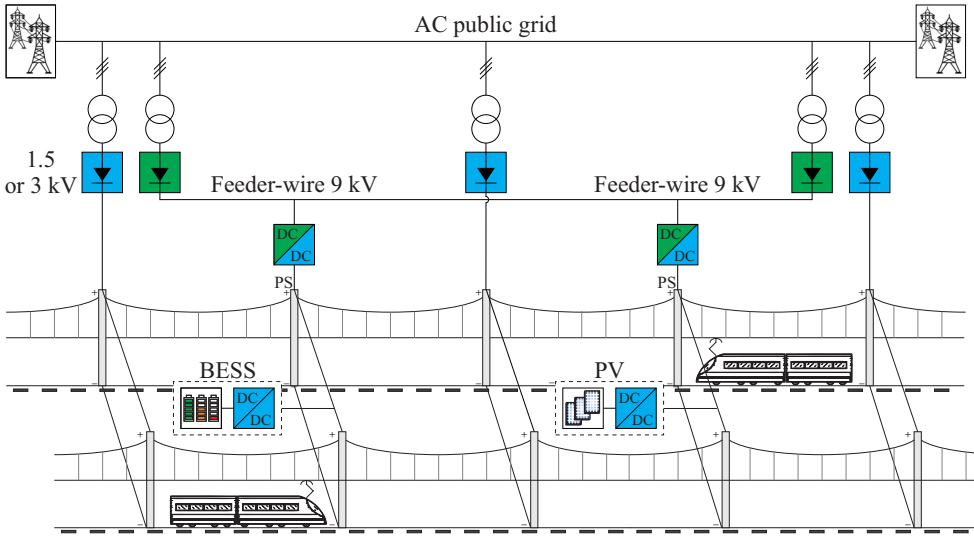

Figure 2. Alternative solutions for reinforcing the DC electrified railways include integrating three-wire DC power feeders, battery energy storage systems and renewable energy sources.

Several works in the literature have proposed incorporating BESS in railway applications [17–21]. Japan railways are the pioneers in this field and have installed around 20 BESS rated at 100 kWh [22,23]. The authors in [24] propose a sizing and control strategy optimization of a hybrid energy storage system based on batteries and ultracapacitors in urban rail transit to reduce the substation energy cost and achieve the peak shaving function. Additionally, the authors in [25] propose a battery and ultracapacitor hybrid storage system for high-speed railway applications. In [26], the impact assessment of energy storage systems supporting DC railways on AC power grids is investigated, considering both wayside and on-board solutions. A techno-economic sizing of auxiliary-battery-based substations in 3 kV Italian DC railway systems is established in [27]. Also, recent research progress and applications of energy storage systems in China's high-speed railways are developed in [28]. However, until now, no BESS has been implemented on the French rail network and there is still no dedicated industrial product.

Therefore, this paper focuses on the sizing of a Modular Battery Energy Storage System (MBESS) based on the association of 300 kW elementary converters, including an isolated DC-DC converter and battery racks. The case studies considered in this paper are for two critical sectors of the French Rail Network where, during peak hour traffic, the contact-line voltage drops below 1.3 kV, limiting the power that the locomotives can draw. Simulations are performed considering real railroad traffic to determine the number of elementary blocks of the MBESS.

This paper is structured as follows: Section 1 introduces the subject of study; Section 2 describes the topology of the MBESS and its control strategy; Section 3 models the railway sector as an equivalent electrical circuit and designs the MBESS for the proposed application. In Section 4, the sizing method is applied for two critical sectors of the French rail network electrified at 1.5 kV. Then, simulation results are presented and discussed. Finally, Section 5 presents the conclusions of the paper and perspectives for future works.

2. Description of the MBESS

2.1. Topology of the Elementary Converter

The topology of the elementary converter is presented in Figure 3. The converter is based on 3.3 kV SiC power modules in LV100 packaging. A Medium Frequency Transformer (MFT) provides galvanic isolation between the railway line and the battery. The Resonant Dual Bridge Converter (RDBC) consists of two H-bridges connected through a series-resonant circuit formed by the MFT's leakage inductances L_p in series with capacitors C_{rp} and C_{rs}. The sizing and the tests of RDBC were presented in papers [29,30]. The resonance

frequency was slightly higher than the switching frequency to obtain a Discontinuous Conduction Mode (DCM) in the AC stage. As a result, the switching losses are very low, which makes it possible to achieve an efficiency of 99% over 80% of the operating range [31]. Conversely, in DCM, the RDBC operates with a constant voltage ratio close to one and therefore does not allow the battery current to be controlled. Thus, a Two-leg Interleaved Step-down Chopper (TISC) regulates the battery current. A coupled inductor (InterCell Transformer, ICT) is connected to the output of the two legs as a solution with reduced volume [32]. The parameters of converters RDBC and TISC as well as the MFT are given in Tables 1 and 2, respectively.

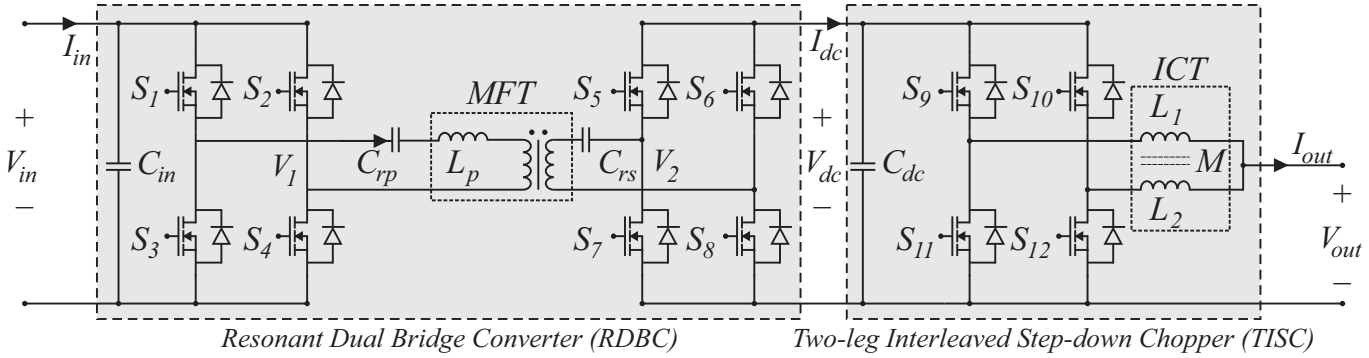

Figure 3. Topology of the SiC-based Isolated DC/DC elementary converter.

Table 1. RDBC and TISC parameters.

Parameters	Symbol	Value
Input voltage range	V_{in}	1.3–1.8 kV
Output voltage range	V_{out}	0.56–1.1 kV
Nominal power	P_n	300 kW
RDBC switching frequency	f_{RDBC}	15 kHz
RDBC resonance frequency	f_0	19.37 kHz
TISC switching frequency	f_{TISC}	7.5 kHz
Input capacitor	C_{in}	60 µF
DC-link capacitor	C_{dc}	120 µF
ICT self-inductance	$L_1 = L_2$	1.35 mH
ICT mutual inductance	M	1 mH

Table 2. MFT parameters.

Parameters	Symbol	Value
Turns ratio	n	1:1
Input voltage range	V_1	1.3–1.8 kV
Nominal power	S_n	400 kVA
Isolation level	V_{iso}	20 kV
Total weight	-	160 kg
Total volume	-	45 L
Cooling system	-	Water (5 L/min)

2.2. Modularity of the BESS

The modularity of the BESS is illustrated in Figure 4. Thanks to the galvanic isolation, several combinations are possible: q is chosen regarding the contact-line voltage and N is determined according to the power or energy required to sustain the traffic on the railway line. The Input Series and Output Parallel (ISOP) association of q elementary converters guarantees a natural balancing of input voltages V_{in} and output currents I_{out}. Additionally, p battery racks can be connected in parallel while respecting the battery's maximum current capability.

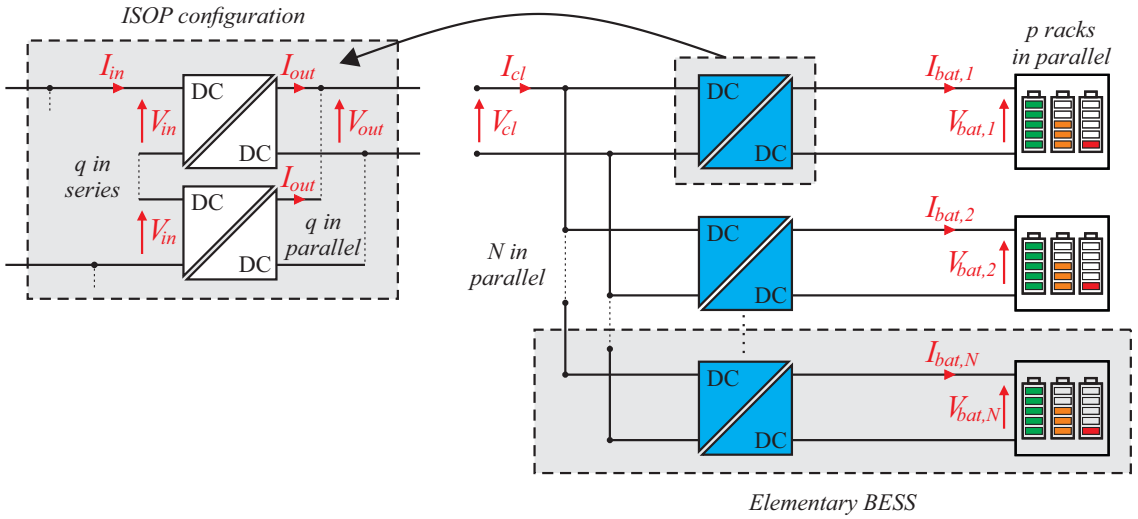

Figure 4. Modularity of the BESS: q elementary converters in series, N elementary BESS in parallel, and battery composed of p racks in parallel.

In RDBC, the isolation of MFT was chosen so that MBESS could be implemented on a future 9 kV electrification system. Table 3 presents the values of q as a function of the nominal voltage level. The voltage ranges for 1.5 kV or 3 kV electrification systems are defined by European standard EN 50163/2005 [33]. The contact-line lowest and highest acceptable voltage V_{cl} during permanent operation are denoted as $V_{cl,min}$ and $V_{cl,max}$, respectively, in this paper. For future MVDC electrification systems, the voltage ranges are defined in [10] while maintaining the same rules of proportionality.

Table 3. Number of elementary converters and battery racks in an MBESS in function of the DC electrification system.

Ref.	Nominal Voltage (kV)	Lowest * Voltage (kV)	Highest * Voltage (kV)	q	p
[33]	1.5	1.0	1.8	1	3
	3.0	2.0	3.6	2	7
[10]	6.0	4.0	7.2	4	14
	9.0	6.0	10.8	6	21

* Permanent operation.

For the first implementation on the French Rail Network, a lithium iron phosphate ($LiFePO_4$ or LFP) battery technology was selected due to safety exigencies. Despite having lower energy density than other battery technologies, the LPF has a longer lifetime and better current/voltage stability [34]. The characteristics of one battery rack are presented in Table 4. The rack is composed of 14 modules in series, thus offering a nominal voltage of 717 V.

Table 4. Characteristics of one battery rack.

Parameters	Symbol	Value
Number of battery modules in series	N_b	14
Nominal voltage	$V_{bat,rack}$	717 V
Nominal capacity	$C_{n,rack}$	120 Ah
Energy	$E_{bat,rack}$	86 kWh
Max. discharge current (1.0 C_n)	$I_{max,d}$	120 A
Max. charge current (0.5 C_n)	$I_{max,c}$	60 A
Depth of Discharge	DoD	>90%

In each BESS, the battery associates p racks in parallel based on the elementary converter nominal output current I_{out}, according to:

$$I_{out,n} = \frac{P_n}{V_{bat,rack}}, \tag{1}$$

$$p = \frac{qI_{out,n}}{I_{max,d}}. \tag{2}$$

2.3. Modelling and Control Strategy of the MBESS

For the sizing of the MBESS, it is necessary to model a railway sector taking into account the movement of trains. The switching period of the converters is negligible compared to the dynamic performances of the trains, thus only an averaged model of the elementary BESS is considered. In Figure 5a, the RDBC is assumed to have a unitary voltage ratio. Then, voltages V_{in} and V_{dc} are supposed to be equal and the input equivalent capacitance C_{eq} is the sum of C_{in} and C_{dc}. The TISC is represented by a small signal model with controlled sources: the current I_{dc} is a function of the output current I_{out} and duty cycle α; the output voltage V_{out} depends on the input voltage V_{in} and also α. The equivalent output inductor L_{eq} corresponds to the leakage inductance of the ICT's windings.

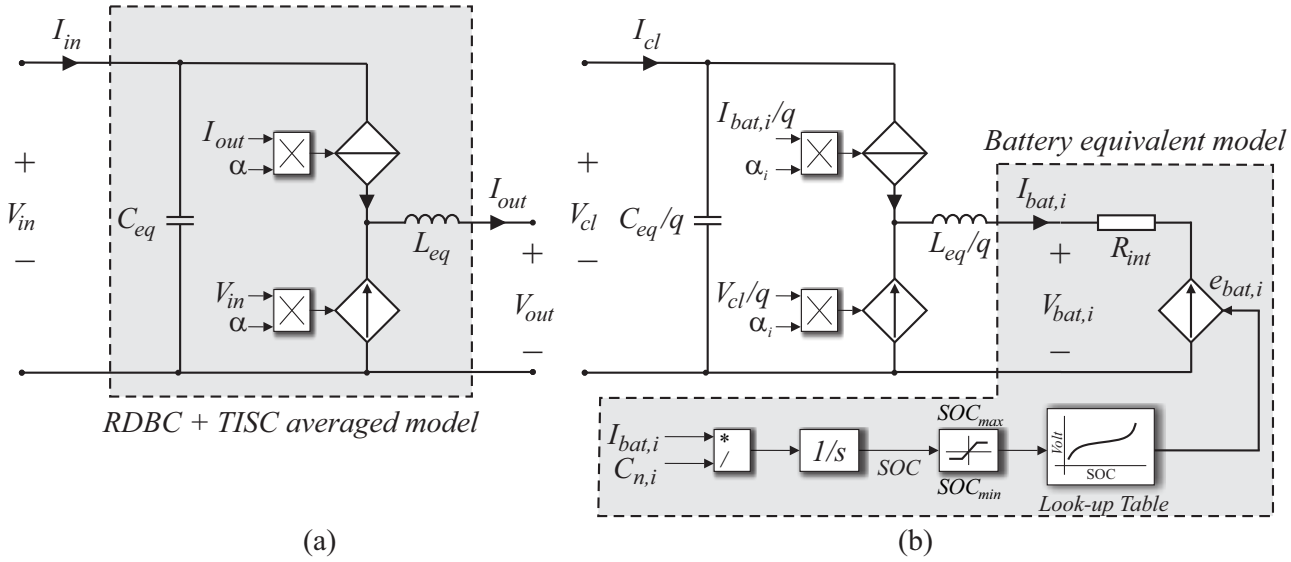

Figure 5. Modeling of the MBESS: (**a**) averaged model of the elementary DC/DC converter; (**b**) averaged model of the MBESS with q elementary blocks connected in ISOP configuration.

The inputs of the elementary converters being connected in series and the outputs in parallel, the averaged model of the elementary BESS, presented in Figure 5b, is easily deduced. Moreover, the battery model is considered as an internal resistance R_{int} in series with an electromotive force $e_{bat,i}$. The values of $e_{bat,i}$ depend on the state of charge (SOC) that is obtained from the integration of the battery current divided by its capacity. A look-up table correlating SOC with battery voltage is provided by the manufacturer.

Figure 6a shows the control block diagram of the MBESS. The inner loops control the battery current whether in charge or discharge mode, for each elementary BESS. The outer loop regulates contact-line voltage V_{cl} at the connection point whose reference value V_{ref} must be carefully determined to maintain the pantograph voltage of the locomotives above a certain level, ensuring correct operation of the trains [35]. The bandwidths of the inner and outer control loops were chosen as 1/10 and 1/100, respectively, of the TISC switching frequency f_{TISC}.

The voltage-current characteristic of MBESS is shown in Figure 6b. When trains are running on the sector and the PI controller of the outer control loop is not saturated,

the MBESS is regulating the contact-line voltage at its connection point, which means that $V_{cl} = V_{ref}$. When the trains pass near this point, the power delivered by the MBESS has to be limited according to the maximum value of the battery discharge current. Thus, the voltage-control loop is disabled (PI controller output saturated at $-I_{max,d}$ and the MBESS operates at negative constant power. Conversely, when the trains are in a regenerative braking phase or when there is no traffic in the sector, the voltage V_{cl} increases and the power absorbed on the contact line by MBESS has to be limited according to the maximal allowed battery charge-current. The outer control loop is again disabled (PI controller output saturated at $I_{max,c}$) and the MBESS operates at positive constant power. The limits of the contact-line voltage, $V_{cl,max}$ and $V_{cl,min}$, depending on the nominal voltage of the electrification system, are given in Table 3. Outside of this voltage range, the MBESS must be disconnected from the contact line by a circuit breaker, as is the case for rolling stock systems.

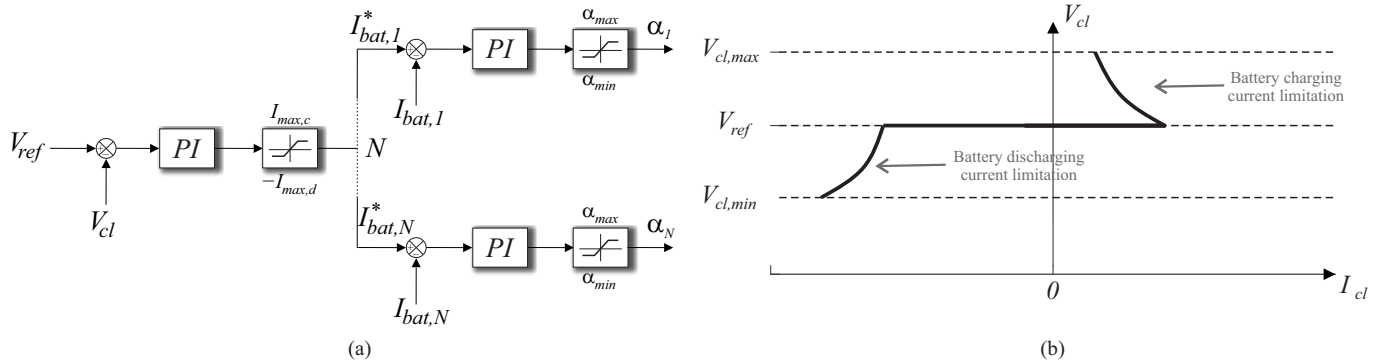

Figure 6. (**a**) Control block diagram of the MBESS and (**b**) MBESS input voltage-current characteristics.

3. Implementation of MBESS on a Railway Sector

3.1. Modeling of a Railway Sector

The railway sector considered in this work consists of a double-track line with a length D and with a PS in the middle of the sector. The MBESS is connected to the already installed PS. The equivalent electrical circuit is presented in Figure 7. The time constants of the electrical circuit are much smaller than the travel time of a train on the sector. Thus, to calculate the voltage at the pantograph of the locomotives, a steady-state DC model is sufficient. Substations at both ends of the sector are modeled as voltage source E_{ss} in series with an internal resistance R_{ss}. The trains are represented as power-controlled current sources according to:

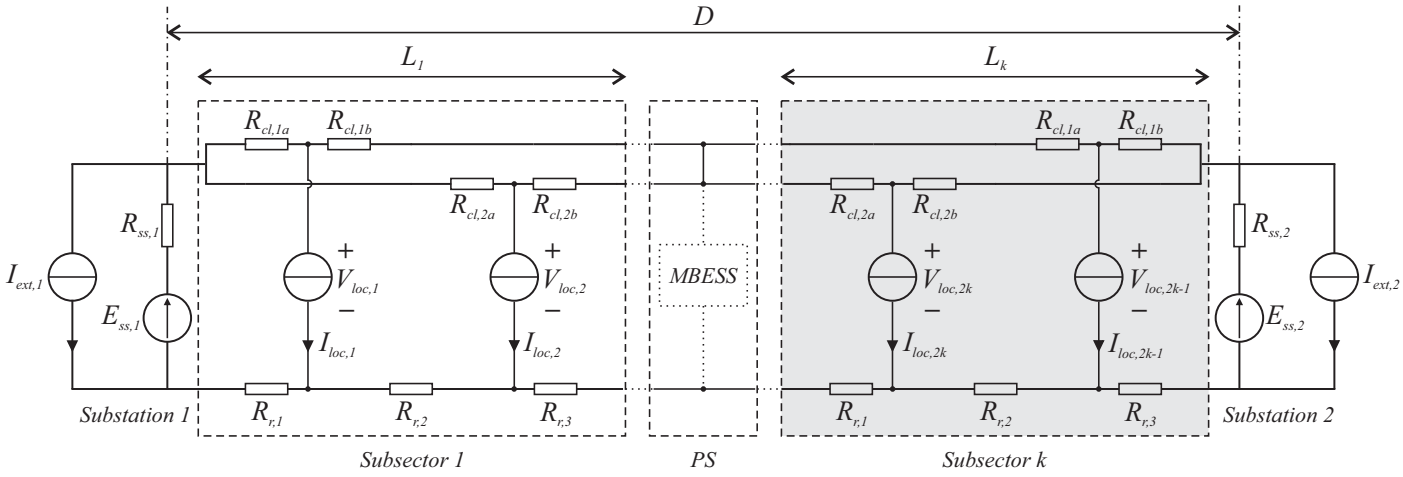

Figure 7. Equivalent circuit of a double-track sector of length D with paralleling station PS at the middle.

$$I_{loc,i} = \frac{P_{loc,i}}{V_{loc,i}}, \tag{3}$$

where $P_{loc,i}$ is the power drawn by the locomotive i and $V_{loc,i}$ and $I_{loc,i}$ correspond to its pantograph voltage and current, respectively. Moreover, $I_{ext,i}$ represents the current circulating outside of the modeled sector, which also has an impact on the pantograph voltage of the trains running on the sector. This information must be provided by the rail network operator.

According to the railroad traffic, this sector is divided into k subsectors with a maximum of one train circulating in each direction at any time. Concerning the numbering of variables, the odd index ($i = 2k - 1$) corresponds to the trains running from left to right while the even index ($i = 2k$) corresponds to the trains running in the opposite direction. If at a given moment, there is no train in circulation in a subsector, the corresponding current source $I_{loc,i}$ is set to zero. Since the rails of the two tracks are electrically connected in parallel at regular intervals, they are considered as a single conductor. The resistances of the contact lines and rails depend on the position of the trains x_{2k} and x_{2k-1}. As can be seen in Figure 8, there are two possible cases of the train's position in each k_{th} subsector. The resistances in the equivalent circuit can be determined by the following equations:

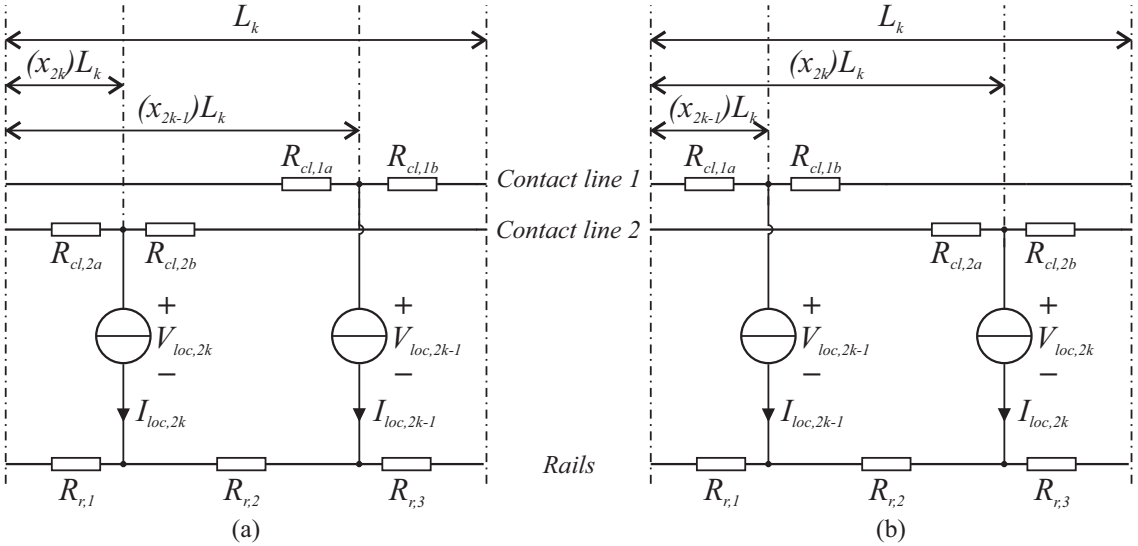

Figure 8. View of the k_{th} subsector of length L_k, considering that in case (**a**) $x_{2k-1} > x_{2k}$, and in case (**b**) $x_{2k} > x_{2k-1}$.

$$R_{cl,1a} = R_a x_{2k-1}, \tag{4}$$

$$R_{cl,1b} = R_a(1 - x_{2k-1}), \tag{5}$$

$$R_{cl,2a} = R_a x_{2k}, \tag{6}$$

$$R_{cl,2b} = R_a(1 - x_{2k}). \tag{7}$$

Considering the case of Figure 8a, when $x_{2k-1} > x_{2k}$, then:

$$R_{r,1} = R_b x_{2k}, \tag{8}$$

$$R_{r,3} = R_b(1 - x_{2k-1}). \tag{9}$$

Similarly, in the case of Figure 8b, when $x_{2k} > x_{2k-1}$, then:

$$R_{r,1} = R_b x_{2k-1}, \tag{10}$$

$$R_{r,3} = R_b(1 - x_{2k}). \tag{11}$$

For both cases, $R_{r,2}$ can be calculated as follows:

$$R_{r,2} = R_b|x_{2k} - x_{2k-1}|. \tag{12}$$

The resistances R_a and R_b are calculated according to:

$$R_a = \frac{18.8}{S_c} L_k, \tag{13}$$

$$R_b = \frac{0.9}{2W_t} L_k, \tag{14}$$

where S_c is the equivalent copper cross-section, expressed in mm², W_t is the weight of the rail per unit length, expressed in kg/m, and L_k is the length of the k_{th} subsector, in km.

3.2. Methodology for Sizing the MBESS

The methodology adopted to correctly size the MBESS is detailed in Figure 9. Three main steps are described regarding the topology of the MBESS that is connected to the PS in the equivalent circuit shown in Figure 7. The data of railroad traffic versus time, i.e., train position $Pk_i(t)$, the power drawn by the train $P_{loc,i}(t)$ and sector external currents $I_{ext,i}(t)$ are considered as inputs of the simulation. The following steps are made, consecutively:

1. Step 1: The first step consists of a railroad traffic preliminary verification. The simulation is performed without the MBESS connected to the PS. Then, over the simulation time horizon, the pantograph voltage $V_{loc,i}$ is compared to a minimum value, $V_{loc,min}$, that avoids a power limitation for the locomotive. European Standard EN 50338/2022 [36] determines technical criteria for traction power supply systems and rolling stock to achieve interoperability following EN 50163/2005 [33]. Usually, this value is around 85% of the contact-line nominal voltage, but it can vary depending on the locomotive manufacturer. If none of the pantograph voltage points are below $V_{loc,min}$, this railroad traffic is considered not critical, thus, there is no need for installing an MBESS. Otherwise, MBESS parameters V_{ref} and N must be determined to maintain the pantograph voltage of the trains above $V_{loc,min}$.
2. Step 2: After establishing the existence of critical points in railroad traffic, the next step is to determine the reference voltage V_{ref} that the MBESS should impose on the contact line. For this, the electrical simulation is performed assuming that MBESS behaves as a voltage source whose value is fixed by the voltage control loop setpoint, V_{ref}, with an initial value of $V_{ref,init} = V_{loc,min}$. Successive simulations are then performed by incrementing V_{ref}, with a ΔV until the following condition is satisfied over the simulation time horizon:

$$V_{loc,i} \geq V_{loc,min}. \tag{15}$$

It should be noted that if the minimum value of V_{ref} that satisfies (15) is equal to or greater than E_{ss}, there is no other solution than to increase the cross-section of the contact line.

3. Step 3: Once V_{ref} is determined, the initial value of N, named as N_{init}, is set according to Equation (16), and rounded to the highest integer value. $P_{MBESS,max}$ is the maximum power supplied by the MBESS when modeled as a controlled voltage source connected at PS (determined in the previous step). P_n is the nominal power of the elementary DC/DC converter given in Table 1 and q is the number of elementary DC/DC converters in ISOP configuration, given in Table 3.

$$N_{init} = \frac{P_{MBESS,max}}{qP_n}. \tag{16}$$

Then, the average model of N MBESS and their control loops are connected at the paralleling station in the equivalent circuit of the sector. The batteries are considered identical and initially fully charged (SOC = 100%). Afterward, successive simulations are performed and N is decremented to satisfy the Equation (15) even in the case of the power delivered by MBESS being limited by the maximum battery discharge current. Minimizing N reduces the installation cost of the MBESS which has to be compared to that of a new substation, which varies greatly with the location of the paralleling station and the need to realize a new AC transmission line to supply the substation.

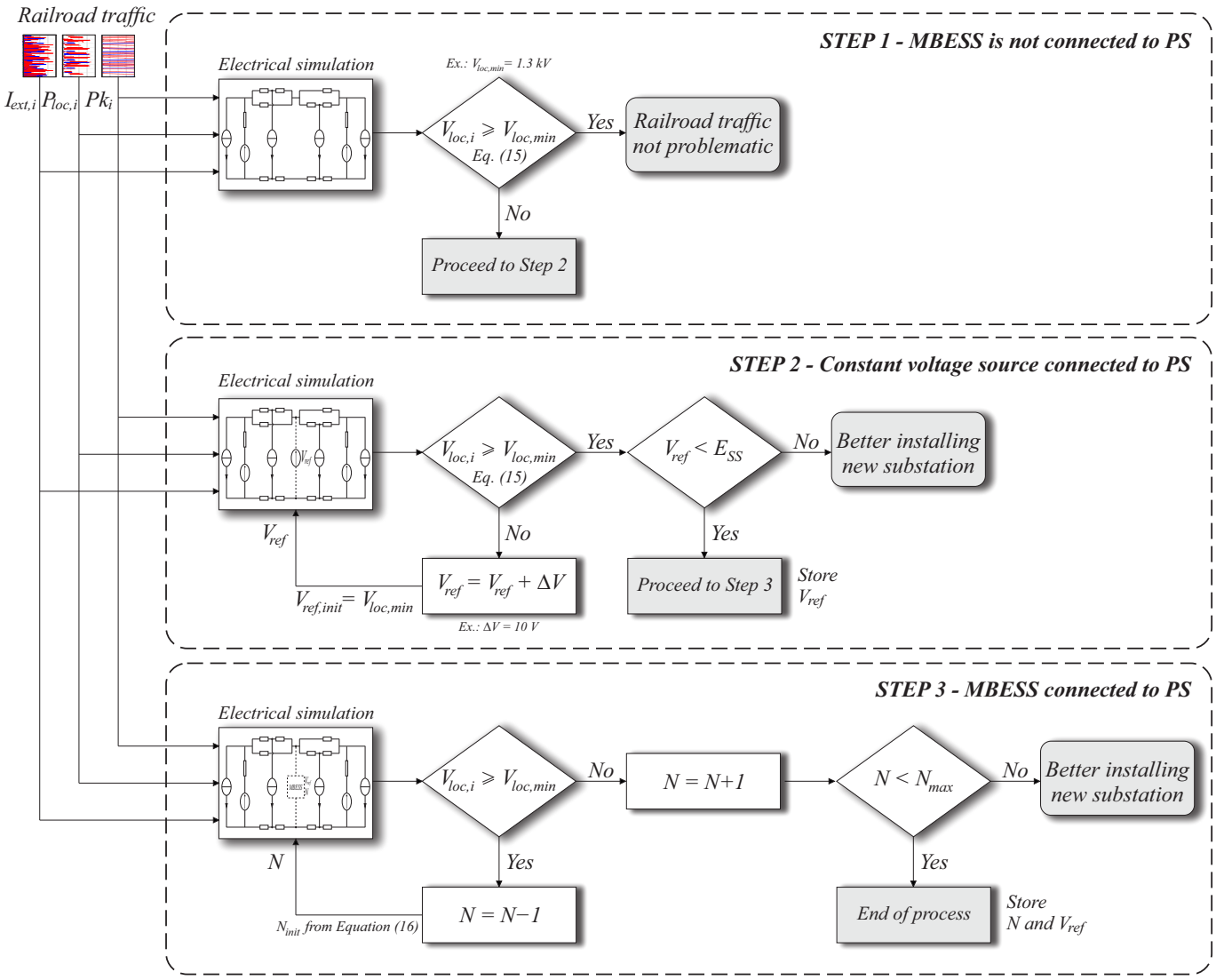

Figure 9. Flowchart of MBESS sizing to find the minimum values of V_{ref} and N that ensures $V_{loc,i} \geq V_{loc,min}$.

4. Sizing of the MBESS—Examples of Sectors on the French Railways

4.1. Description of the Railway Sectors

This section applies the proposed methodology to size the MBESS for two different sectors on the French Rail Network. These sectors are electrified in 1.5 kV DC both consisting of a double-track line with trains circulating in each direction, as illustrated in Figure 10. The simulation of the equivalent circuit presented in Figure 7 is performed on PLECS software, version 4.8.1 (64 bits) [37], considering that the MBESS is installed at a PS.

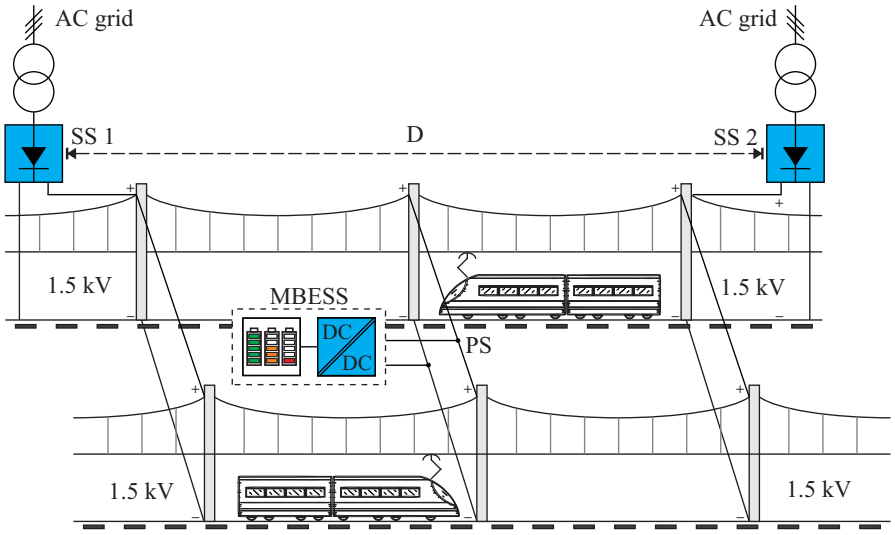

Figure 10. Representation of the railway sector provided by SNCF-Réseau. It consists of a double-track sector with trains circulating in each direction.

The first railway sector is located on the Lyon-Dijon classical line between the substations of Crèches (Pk = 445 km) and Romanèche (Pk = 453 km), with a paralleling station at the sector midpoint (Pk = 449 km). The second sector is located on the Chartres-Le Mans regional line between the substations of Le Theil (Pk = 159 km) and Sceaux-Boëssé (Pk = 179 km), with a paralleling station also positioned in the middle of the sector (Pk = 169 km). From the point of view of the French Rail Network Operator (SNCF-Réseau), these sectors are considered problematic because significant contact-line voltage drops occur.

Table 5 specifies the parameters used in the simulations for both cases. Because of the paralleling station, there are always, at least two subsectors. Nevertheless, the number of subsectors in the equivalent circuit can be chosen according to the railroad traffic. Thus, with four subsectors it is possible to have simultaneously in the sector, a maximum of four trains circulating in each direction.

Table 5. Parameters of the two railway sectors investigated in the case study.

Crèches-Romanèche Sector		
Parameter	**Symbol**	**Value**
Substation spacing	D	8 km
Number of subsectors	k	2
Substation 1 no-load voltage	$E_{ss,1}$	1750 V
Substation 1 internal resistance	$R_{ss,1}$	28 mΩ
Substation 2 no-load voltage	$E_{ss,2}$	1750 V
Substation 2 internal resistance	$R_{ss,2}$	28 mΩ
Contact-line cross-section	S_c	432 mm²
Rail weight per unit length	W_t	50 kg/m²
Le Theil-Sceaux-Boëssé sector		
Parameter	Symbol	Value
Substation spacing	D	19.4 km
Number of subsectors	k	4
Substation 1 no load voltage	$E_{ss,1}$	1750 V
Substation 1 internal resistance	$R_{ss,1}$	21 mΩ
Substation 2 no load voltage	$E_{ss,2}$	1750 V
Substation 2 internal resistance	$R_{ss,2}$	70 mΩ
Contact-line cross-section	S_c	368 mm²
Rail weight per unit length	W_t	60 kg/m²

The information required for the simulations, $Pk_i(t)$, $P_{loc,i}(t)$, $I_{ext,1}(t)$ and $I_{ext,2}(t)$, was provided by SNCF-Réseau. The time plots for the sectors Crèches-Romanèche and Le Theil-Sceaux-Boëssé are shown in Figure 11. The time interval considered corresponds to a traffic peak in the sector.

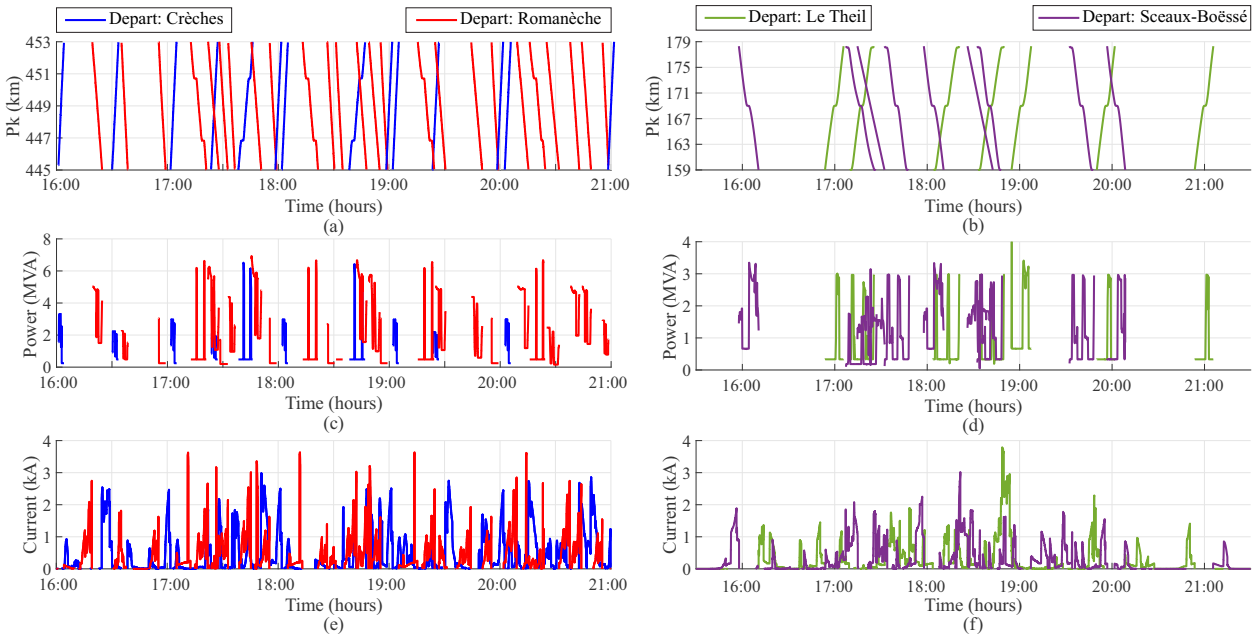

Figure 11. Railroad traffic between the substations of Crèches-Romanèche (left side) and Le Theil-Sceaux-Boëssé (right side): (**a**,**b**) Pk, (**c**,**d**) P_{loc}, (**e**,**f**) I_{ext}.

Table 6 presents a preliminary analysis of traffic in the considered sectors. The Crèches-Romanèche sector has the shortest length and the critical situation results from high power train circulations with a high traffic density. Regarding the Le Theil-Sceaux-Boëssé sector, the critical situation results from greater substation spacing and a low contact-line cross-section. Even though the trains draw less power than in the previous sector, the energy demand is increased because the travel time to cross the sector is longer.

Table 6. Preliminary assessment of traffic in each sector from 16:00 to 21:00.

Parameters	Crèches-Romanèche	Le Theil-Sceaux-Boëssé
Number of trains running from left to right	10	7
Number of trains running from right to left	25	9
Average travel time from left to right	4.27 min	14.16 min
Average travel time from right to left	5.29 min	15.47 min
Mean of the averaged power drawn from trains running from left to right	1.44 MW	0.85 MW
Mean of the averaged power drawn from trains running from right to left	1.90 MW	1.23 MW
Average value of the energy absorbed by trains running from left to right	94.86 kWh	200.41 kWh
Average value of the energy absorbed by trains running from right to left	171.06 kWh	312.71 kWh

4.2. Simulation Results of the MBESS Boosting the Locomotives Pantograph Voltage

Figures 12a,b and 13a,b show the pantograph voltage of the locomotives over Pk for both sectors before the installation of the MBESS. In the following analysis, $V_{loc,min}$ = 1.3 kV will be considered as the threshold voltage for critical points. Therefore, operating points with a voltage below 1.3 kV are observed in both cases. In such a situation, the operation of locomotives at constant power can be constrained by the limitation of the current absorbed by the traction inverters, leading to delays and disturbances in the railroad traffic. Therefore, the MBESS is installed in this sector to reinforce the power supply and avoid pantograph

voltage values lower than 1.3 kV. The MBESS sizing process, presented in Figure 9, was applied for both sectors, and Table 7 shows the corresponding values of N and V_{ref}. Since the railway sector is electrified in 1.5 kV DC, q and p are selected as 1 and 3, respectively, according to Table 3.

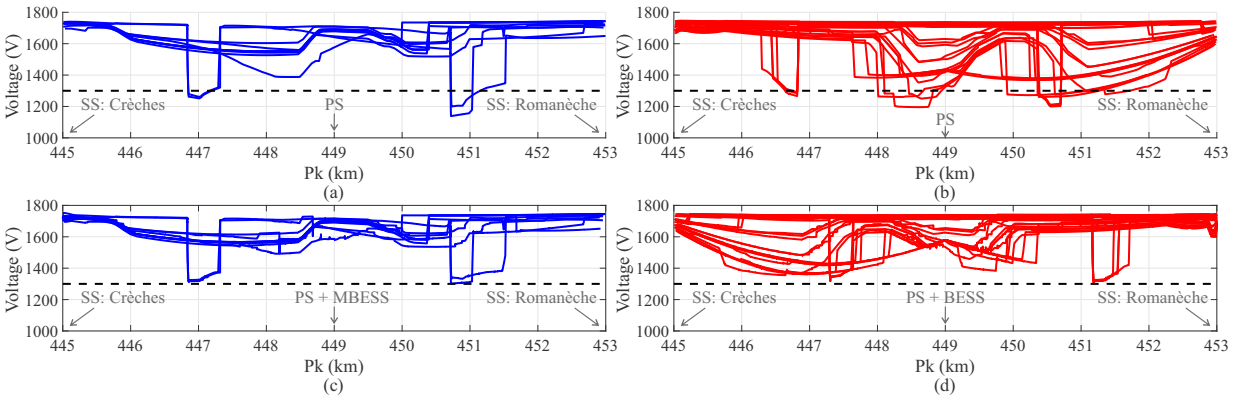

Figure 12. Pantograph voltage of the locomotives before (upside) and after (downside) the installation of the MBESS on the railway sector: (**a**,**c**) trains departing from Crèches; (**b**,**d**) trains departing from Romanèche.

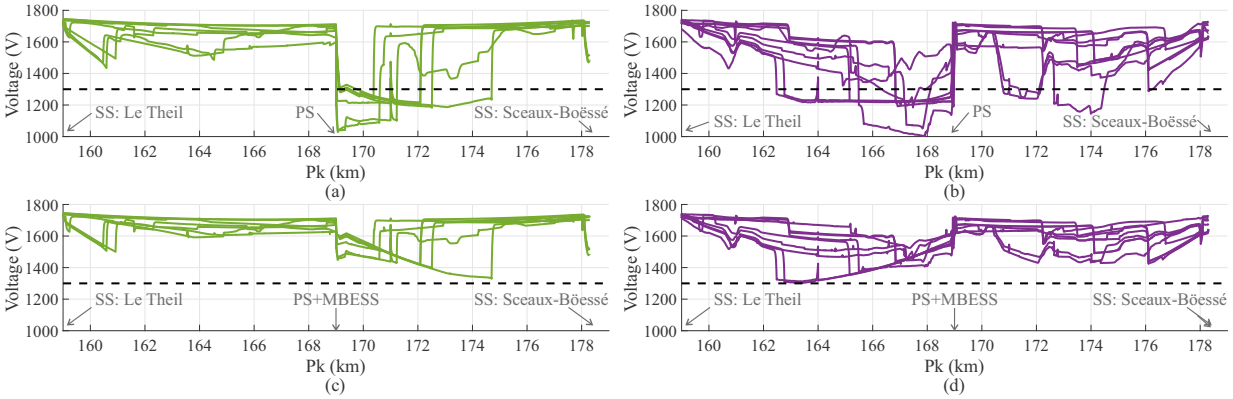

Figure 13. Pantograph voltage of the locomotives before (upside) and after (downside) the installation of the MBESS on the railway sector: (**a**,**c**) trains departing from Le Theil; (**b**,**d**) trains departing from Sceaux-Boëssé.

Table 7. Sizing parameters of the MBESS.

Parameter	Crèches-Romanèche	Le Theil-Sceaux-Boëssé
N	10	8
V_{ref}	1580 V	1630 V

Figures 12c,d and 13c,d show the pantograph voltage of the locomotives over Pk for both sectors after the installation of the MBESS. As can be noticed, the critical points have been removed. Figure 14 shows a time-zoomed view of the action of the MBESS in the first case study, due to the passage of a freight train with two high-power peaks. During the first power peak, the MBESS regulates the voltage at PS to V_{ref} (Voltage Source Mode: VSM). During the second power peak, the discharge current of the batteries is limited. In this case, the MBESS behaves as a current source operating at constant power (Current Source Mode: CSM). Nevertheless, the contact-line voltage is still maintained above 1.3 kV. Figure 15a presents the contact-line characteristics of V_{cl} *versus* I_{cl} over the simulation time horizon of the Crèches-Romanèche case study, as an example. When comparing the contact-line operation points with Figure 6b, it is possible to identify the zone of VSM with V_{cl} regulated at 1580 V and the zones of CSM, with battery charge and discharge saturation.

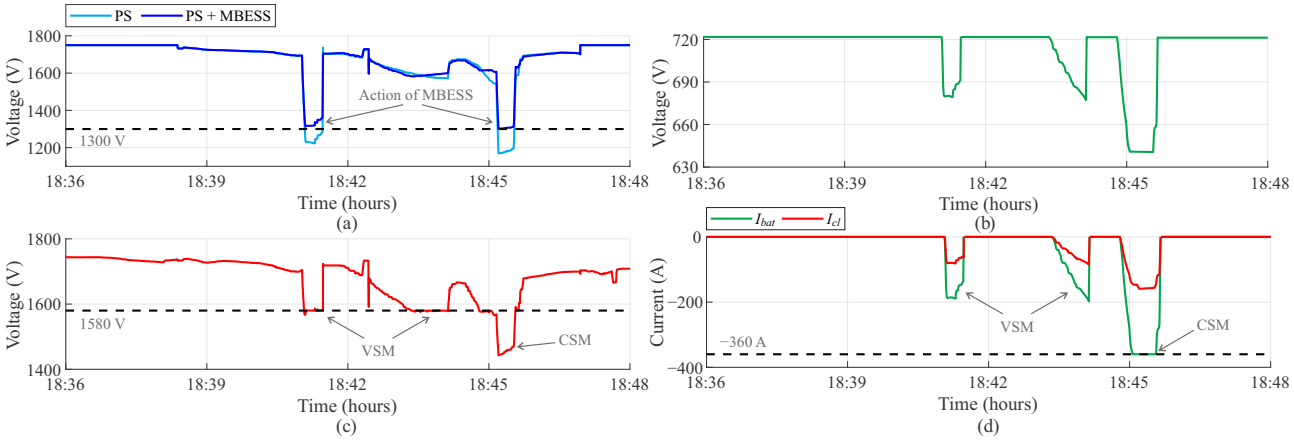

Figure 14. Time-zoomed view between 18:36 and 18:48 hours during a freight train passage with two high-power peaks departing from Crèches: (**a**) pantograph voltage of the locomotive V_{loc}; (**b**) battery rack voltage V_{bat}, (**c**) contact-line voltage V_{cl} at PS; and (**d**) contact-line current I_{cl} at PS and battery current I_{bat}. Remark: $q = 1$ and $p = 3$.

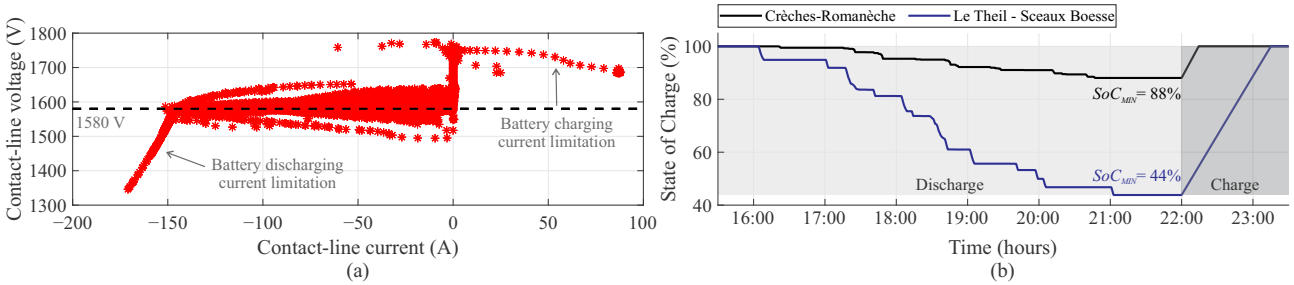

Figure 15. (**a**) Simulated characteristic of contact-line voltage V_{cl} *versus* contact-line current I_{cl} obtained from simulation over the time horizon of case study Crèches-Romanèche; (**b**) MBESS state-of-charge at the end of peak traffic. From 16:00 to 21:00, the batteries are discharged to supply the trains. After 22:00, the batteries are recharged to 100%.

With $N = 10$ in the first case, the total storage energy capacity is 2.58 MWh, higher than the second case with $N = 8$, storing 2.06 MWh. In this study, the decision to only charge the MBESS in the off-peak traffic period was taken. Thus, during the time interval 16:00–21:00, the MBESS is only discharging. After 22:00 there are no trains in circulation and the substations charge the batteries. Figure 15b shows the state-of-charge (SOC) of the batteries for both analyzed sectors.

In the case study Crèches - Romanèche, the battery SOC is reduced from 100% to 88%. The energy storage is much higher than that needed. In fact, the MBESS mostly provides current to the sector to compensate for the high-power-demand trains, but only for a short period, due to the short length of the sector. After 22:00, the MBESS batteries are recharged to 100% at current $I_{max,c}$ in around 15 min. In the case of Le Theil-Sceaux-Boëssé, after the traffic peak, the SOC of the batteries decreases to 44%. Due to the higher sector length, the batteries must deliver power over a longer time. After 22:00, MBESS batteries are recharged to 100% at current $I_{max,c}$ in around 1 h 30 min.

In the two sectors studied, it is important to note that the total depth of discharge is never reached. In fact, as it was presented in Section 2, the number of battery racks depends on the current rating of the elementary power converter. Additionally, according to the sizing process shown in Figure 9, N is selected to provide the peak power required to ensure a pantograph voltage above $V_{loc,min}$ = 1.3 kV. Therefore, due to the characteristics of the selected battery, the stored energy is always oversized.

4.3. Impact of the MBESS on the Global System Efficiency

The elimination of critically low values of locomotive pantograph voltage is not the only advantage of installing an MBESS. Along the sector, the locomotives operate with a higher contact-line voltage and consequently draw a lower current. Therefore, there is an improvement in the global electrical system efficiency because of the lower power losses in the contact line and the rails. Tables 8 and 9 show the energy balance of the sector before and after the installation of an MBESS for each case of study. The energy absorbed by the trains does not change from one condition to another, as it depends exclusively on the traffic. However, the substations provide less current due to the reduced voltage drop along the contact lines. The energy provided by the batteries to the railway line takes into account the SOC reduction previously calculated and the losses in the internal resistor R_{int}. However, the losses in the power converters are not considered. The energy efficiency of the railway sector is calculated over the simulation time according to Equation (17) where $E_{loc,i}$ is the energy consumed by the trains running on the sector and $E_{sub,i}$ is the energy provided by the substations, also allowing for the energy required to recharge the battery to 100% of capacity. As noticed, there is a gain of around 2% in efficiency with the installation of the MBESS for both cases, which is very relevant considering the power level of the railway application.

$$\eta_{global} = \left(\frac{E_{loc,1} + E_{loc,2}}{E_{sub,1} + E_{sub,2}} \right) 100\%. \tag{17}$$

Table 8. Crèches-Romanèche railway sector energy balancing before and after the installation of the MBESS.

Parameters	Symbol	Initial Situation	After MBESS Installation
Sum of energies absorbed by trains running from Crèches to Romanèche	$E_{loc,1}$	0.95 MWh	0.95 MWh
Sum of energies absorbed by trains running from Romanèche to Crèches	$E_{loc,2}$	4.28 MWh	4.28 MWh
Total energy provided by the substation at Crèches	$E_{sub,1}$	2.60 MWh	2.51 MWh
Total energy provided by the substation at Romanèche	$E_{sub,2}$	3.35 MWh	3.30 MWh
Energy efficiency	η_{global}	87.90%	90.02%

Table 9. Le Theil-Sceaux-Boëssé railway sector energy balancing before and after the installation of the MBESS.

Parameters	Symbol	Initial Situation	After MBESS Installation
Sum of energies absorbed by trains running from Le Theil to Sceaux-Boëssé	$E_{loc,1}$	1.40 MWh	1.40 MWh
Sum of energies absorbed by trains running from Sceaux-Boëssé to Le Theil	$E_{loc,2}$	2.82 MWh	2.82 MWh
Total energy provided by the substation at Le Theil	$E_{sub,1}$	2.84 MWh	2.75 MWh
Total energy provided by the substation at Sceaux-Boëssé	$E_{sub,2}$	2.21 MWh	2.17 MWh
Energy efficiency	η_{global}	83.56%	85.77%

5. Conclusions

This paper proposed a modular BESS solution to reinforce DC railway lines. By reducing the contact-line voltage drop, the MBESS prevents the onboard locomotive control system from limiting the traction power. Therefore, trains can respect their timetables. Furthermore, the power losses in the contact line and the rails are reduced and the energy efficiency of the electrification system is improved. Thanks to the galvanic isolation included in the DC/DC converters, the solution is suitable for different contact-line voltage levels, including for future 6 kV or 9 kV electrified lines still under consideration.

The sizing method of the MBESS was presented in Section 3. The number of elementary blocks depends on the electrical parameters of the sector considered and the rail traffic. To run the simulations, traffic information, and power consumed by trains must be provided by the rail infrastructure manager. The two case studies covered in this paper were provided by SNCF-Réseau, the French rail infrastructure manager. The first one concerns a sector

of a main line where there is a high traffic density with high-power trains in circulation. The second one concerns a sector of a regional line with large substation spacing and a low contact-line cross-section. Respectively, the power ratings of the MBESS are 3 MW and 2.4 MW which represents about half of the nominal power of a substation used on lines electrified in 1.5 kV DC.

Taking into account the characteristics of the batteries initially selected, the stored energies are 2.58 MWh and 2.06 MWh. These values are oversized regarding the evolution of the battery SOC during the peaks of traffic. A way of optimizing the storage energy and the power capability of the MBESS could be simply increasing the battery's nominal voltage. However, this is problematic given the battery management system currently available.

Finally, it is important to say that the work presented here is the design of a planned prototype to be installed on a line of the French rail network. Further studies are expected to achieve the integration of the MBESS in the railway line, design of input filters, different energy management strategies, lifetime evaluations and so on.

Author Contributions: Conceptualization, P.L. and J.F.; methodology, E.M.d.S.B. and P.L.; validation, E.M.d.S.B. and B.S.; writing and editing, E.M.d.S.B. and P.L.; review, J.F. and B.S. All authors have read and agreed to the published version of the manuscript.

Funding: This research was carried out as part of the INSTODRES project. INSTODRES is funded by the French Government as part of the Investment Program "France 2030", and operated by French Agency for Ecological Transition (ADEME) (2105D0041).

Data Availability Statement: The data presented in this study are available on request from the corresponding author.

Conflicts of Interest: Author Joseph Fabre was employed by the company SCLE-SFE. Author Benoit Sonier was employed by the company French National Railway Company (SNCF) Réseau. The remaining authors declare that the research was conducted in the absence of any commercial or financial relationships that could be construed as a potential conflict of interest.

Abbreviations

The following abbreviations are used in this manuscript:

AC	Alternating Current
BESS	Battery Energy Storage System
CSM	Current Source Mode
DC	Direct Current
DCM	Discontinuous Conduction Mode
DoD	Depth of Discharge
EN	European Standard
EU	European Union
ICT	Intercell Transformer
ISOP	Input Series and Output Parallel
LFP	Lithium Iron Phosphate
MBESS	Modular Battery Energy Storage System
MFT	Medium Frequency Transformer
MVAC	Medium Voltage AC
MVDC	Medium Voltage DC
PI	Proportional Integral controller
PLECS	Piecewise Linear Electrical Circuit Simulation
PS	Paralleling Station
PV	Photovoltaic
RDBC	Resonant Dual Bridge Converter
SiC	Silicon Carbide
SOC	State of charge
SNCF	Société Nationale des Chemins de Fer Français
TISC	Two-leg Interleaved Step-down Chopper
VSM	Voltage Source Mode

References

1. *IEC 60850*; Railway Applications-Supply Voltages of Traction Systems. International Electrotechnical Commission: Geneva, Switzerland, 2014.
2. Bueker. Maps and Facts on European Interoperability Issues. Available online: http://www.bueker.net/trainspotting/voltage_map_europe.php (accessed on 26 March 2018).
3. CER. Railway to a Green Future. Available online: https://www.cer.be/cer-facts-figures/railway-to-a-green-future (accessed on 4 December 2023).
4. Steimel, A. Under Europe's incompatible catenary voltages a review of multi-system traction technology. In Proceedings of the 2012 Electrical Systems for Aircraft, Railway and Ship Propulsion, Bologna, Italy, 16–18 October 2012; pp. 1–8. [CrossRef]
5. Mousavi Gazafrudi, S.M.; Tabakhpour Langerudy, A.; Fuchs, E.F.; Al-Haddad, K. Power Quality Issues in Railway Electrification: A Comprehensive Perspective. *IEEE Trans. Ind. Electron.* **2015**, *62*, 3081–3090. [CrossRef]
6. He, X.; Peng, J.; Han, P.; Liu, Z.; Gao, S.; Wang, P. A Novel Advanced Traction Power Supply System Based on Modular Multilevel Converter. *IEEE Access* **2019**, *7*, 165018–165028. [CrossRef]
7. Gómez-Expósito, A.; Mauricio, J.M.; Maza-Ortega, J.M. VSC-Based MVDC Railway Electrification System. *IEEE Trans. Power Deliv.* **2014**, *29*, 422–431. [CrossRef]
8. Zhu, R.; Liang, T.; Dinavahi, V.; Liang, G. Wideband Modeling of Power SiC mosfet Module and Conducted EMI Prediction of MVDC Railway Electrification System. *IEEE Trans. Electromagn. Compat.* **2020**, *62*, 2621–2633. [CrossRef]
9. Yang, X.; Hu, H.; Ge, Y.; Aatif, S.; He, Z.; Gao, S. An Improved Droop Control Strategy for VSC-Based MVDC Traction Power Supply System. *IEEE Trans. Ind. Appl.* **2018**, *54*, 5173–5186. [CrossRef]
10. Verdicchio, A.; Ladoux, P.; Caron, H.; Courtois, C. New Medium-Voltage DC Railway Electrification System. *IEEE Trans. Transp. Electrif.* **2018**, *4*, 591–604. [CrossRef]
11. Ladoux, P.; Blaquiere, J.M.; Caron, H.; Iannuzzi, D.; Coppola, M. New three-wire supply systems for DC electric railways. *IET Electr. Syst. Transp.* **2015**, *5*, 112–119. [CrossRef]
12. Dong, H.; Tian, Z.; Spencer, J.W.; Fletcher, D.; Hajiabady, S. Coordinated Control Strategy of Railway Multisource Traction System With Energy Storage and Renewable Energy. *IEEE Trans. Intell. Transp. Syst.* **2023**, *24*, 15702–15713. [CrossRef]
13. Aatif, S.; Yang, X.; Hu, H.; Maharjan, S.K.; He, Z. Integration of PV and Battery Storage for Catenary Voltage Regulation and Stray Current Mitigation in MVDC Railways. *J. Mod. Power Syst. Clean Energy* **2021**, *9*, 585–594. [CrossRef]
14. Liu, X.; Li, K. Energy storage devices in electrified railway systems: A review. *Transp. Saf. Environ.* **2020**, *2*, 183–201. [CrossRef]
15. Hu, X.; Deng, X.; Wang, F.; Deng, Z.; Lin, X.; Teodorescu, R.; Pecht, M.G. A Review of Second-Life Lithium-Ion Batteries for Stationary Energy Storage Applications. *Proc. IEEE* **2022**, *110*, 735–753. [CrossRef]
16. Walvekar, H.; Beltran, H.; Sripad, S.; Pecht, M. Implications of the Electric Vehicle Manufacturers' Decision to Mass Adopt Lithium-Iron Phosphate Batteries. *IEEE Access* **2022**, *10*, 63834–63843. [CrossRef]
17. Lee, H.M. A study on development of ESS installed in DC railway system. In Proceedings of the ICCAS 2010, Goyang-si, Republic of Korea, 27–30 October 2010; pp. 804–806. [CrossRef]
18. Ahmadi, M.; Jafari Kaleybar, H.; Brenna, M.; Castelli-Dezza, F.; Carmeli, M.S. Integration of Distributed Energy Resources and EV Fast-Charging Infrastructure in High-Speed Railway Systems. *Electronics* **2021**, *10*, 2555. [CrossRef]
19. Ratniyomchai, T.; Kulworawanichpong, T. A Demonstration Project for Installation of Battery Energy Storage System in Mass Rapid Transit. *Energy Procedia* **2017**, *138*, 93–98. [CrossRef]
20. Lamedica, R.; Ruvio, A.; Galdi, V.; Graber, G.; Sforza, P.; GuidiBuffarini, G.; Spalvieri, C. Application of battery auxiliary substations in 3kV railway systems. In Proceedings of the 2015 AEIT International Annual Conference (AEIT), Naples, Italy, 14–16 October 2015; pp. 1–6. [CrossRef]
21. Calderaro, V.; Galdi, V.; Graber, G.; Piccolo, A.; Capasso, A.; Lamedica, R.; Ruvio, A. Energy management of Auxiliary Battery Substation supporting high-speed train on 3 kV DC systems. In Proceedings of the 2015 International Conference on Renewable Energy Research and Applications (ICRERA), Palermo, Italy, 22–25 November 2015; pp. 1224–1229. [CrossRef]
22. Konishi, T.; Morimoto, H.; Aihara, T.; Tsutakawa, M. Fixed Energy Storage Technology Applied for DC Electrified Railway. *IEEJ Trans. Electr. Electron. Eng.* **2010**, *5*, 270–277. [CrossRef]
23. Konishi, T.; Tobita, M. Fixed energy storage technology applied for DC electrified railway (traction power substation). In Proceedings of the 2012 Electrical Systems for Aircraft, Railway and Ship Propulsion, Bologna, Italy, 16–18 October 2012; pp. 1–6. [CrossRef]
24. Dong, H.; Tian, Z.; Spencer, J.W.; Fletcher, D.; Hajiabady, S. Bi-level Optimization of Sizing and Control Strategy of Hybrid Energy Storage System in Urban Rail Transit Considering Substation Operation Stability. *IEEE Trans. Transp. Electrif.* **2024**. [CrossRef]
25. de la Torre, S.; Sánchez-Racero, A.J.; Aguado, J.A.; Reyes, M.; Martínez, O. Optimal Sizing of Energy Storage for Regenerative Braking in Electric Railway Systems. *IEEE Trans. Power Syst.* **2015**, *30*, 1492–1500. [CrossRef]
26. Graber, G.; Calderaro, V.; Galdi, V.; Ippolito, L.; Massa, G. Impact Assessment of Energy Storage Systems Supporting DC Railways on AC Power Grids. *IEEE Access* **2022**, *10*, 10783–10798. [CrossRef]
27. Graber, G.; Calderaro, V.; Galdi, V.; Piccolo, A.; Lamedica, R.; Ruvio, A. Techno-economic Sizing of Auxiliary-Battery-Based Substations in DC Railway Systems. *IEEE Trans. Transp. Electrif.* **2018**, *4*, 616–625. [CrossRef]
28. Yuan, J.; Peng, L.; Zhou, H.; Gan, D.; Qu, K. Recent research progress and application of energy storage system in electrified railway. *Electr. Power Syst. Res.* **2024**, *226*, 109893. [CrossRef]

29. Fabre, J.; Ladoux, P.; Caron, H.; Verdicchio, A.; Blaquière, J.M.; Flumian, D.; Sanchez, S. Characterization and Implementation of Resonant Isolated DC/DC Converters for Future MVdc Railway Electrification Systems. *IEEE Trans. Transp. Electrif.* **2021**, *7*, 854–869. [CrossRef]
30. Fortes, G.; Ladoux, P.; Fabre, J.; Flumian, D. Characterization of a 300 kW Isolated DCDC Converter using 3.3 kV SiC-MOSFETs. In Proceedings of the PCIM Europe digital days 2021; International Exhibition and Conference for Power Electronics, Intelligent Motion, Renewable Energy and Energy Management, Online, 3–7 May 2021; pp. 1–8.
31. Hannan, M.A.; Ker, P.J.; Lipu, M.S.H.; Choi, Z.H.; Rahman, M.S.A.; Muttaqi, K.M.; Blaabjerg, F. State of the Art of Solid-State Transformers: Advanced Topologies, Implementation Issues, Recent Progress and Improvements. *IEEE Access* **2020**, *8*, 19113–19132. [CrossRef]
32. Laboure, E.; Cuniere, A.; Meynard, T.A.; Forest, F.; Sarraute, E. A Theoretical Approach to InterCell Transformers, Application to Interleaved Converters. *IEEE Trans. Power Electron.* **2008**, *23*, 464–474. [CrossRef]
33. *EU 50163/2005*; Railway Applications-Supply Voltages of Traction Systems. European Standard: Geneva, Switzerland, 2005.
34. Kim, H.J.; Krishna, T.; Zeb, K.; Rajangam, V.; Gopi, C.V.V.M.; Sambasivam, S.; Raghavendra, K.V.G.; Obaidat, I.M. A Comprehensive Review of Li-Ion Battery Materials and Their Recycling Techniques. *Electronics* **2020**, *9*, 1161. [CrossRef]
35. Fabre, J.; Ladoux, P.; Caron, H. Fixed (Trackside) Energy Storage System for DC Electric Railways Based on Full-SiC Isolated DC-DC Converters. *Electronics* **2023**, *12*, 1675. [CrossRef]
36. *EU 50338/2022*; Railway Applications-Fixed Installations and Rolling Stock-Technical Criteria for the Coordination between Electric Traction Power Supply Systems and Rolling Stock to Achieve Interoperability—Part 1: General. European Standard: Geneva, Switzerland, 2022.
37. Plexim. *PLECS The Simulation Platform for Power Electronic Systems*; Technical Report; Plexim: Zurich, Switzerland, 2024.